J. Meas. Sci. Instrum., 2025, 16(3): 415-424.
DOI: 10.62756/jmsi.1674-8042.2025040
http://jmsi.publish.founderss.cn/
jmsi@nuc.edu.cn

Improved virtual DC generator technique for PV power generation units in railway field

ZHAO Feng, XIAO Chengrui*, CHEN Xiaoqiang, WANG Ying
School of Automation and Electrical Engineering, Lanzhou Jiaotong University, Lanzhou 730070, China

***Corresponding author:** XIAO Chengrui (3206906420@qq.comn)

Received: August 16, 2024 **Revised:** September 21, 2024 **Accepted:** September 24, 2024

Abstract: The power-electronics-based DC microgrid system composed of new energy sources in railway field has low inertia, weak damping characteristics, and the voltage fluctuation microgrid systems caused by the power disturbance of solar. In order to improve the inertia of the DC microgrid system, a virtual DC generator technology is adopted in the interface converter of photovoltaic (PV) power generation unit, so that it has the external characteristics of DC generator. However, the influence of PV maximum power point tracking (MPPT) is not considered in the traditional virtual DC generator control. Therefore, an improved control strategy for virtual DC generator is proposed, and its small signal model is established to analyze the influence of inertia and damping coefficient on stability. The results show that the proposed method effectively weakens the impact on DC bus voltage when the output of PV power unit changes suddenly, which improves the stability of the microgrid. Meanwhile, the correctness and feasibility of the method are verified.

Key words: renewable energy; photovoltaic (PV) system; power-electronics-based DC microgrid system; virtual DC generator control; virtual inertia

0 Introduction

With the increasing improvement of China's railway network, there has been an increasingly growing tendency for the electricity consumption, which gives the opportunity that the renewable energy represented by solar energy can be widely applied in the non-traction field of electrified railway[1]. Meanwhile, compared with AC microgrid, DC microgrid has become one of the research hotspots in recent years because of simple control, high reliability and no reactive power component, harmonics and other problems[2]. Therefore, in the DC microgrid system composed of solar and storage energy sources of railway field, the bus voltage is considered as precondition to support system stability[3]. A large number of power electronic converters that have the characteristics of rapid action and flexible control are used in solar-storage DC microgrid system for railway field, which will lead to the lack of inertia and damping[4]. Thus, the power supply quality is easy to be seriously affected by photovoltaic (PV) output power due to the fluctuations of external environment. However, many solutions have been proposed by scholars to solve the problems of lack of inertia and damping in power electronic system. Chai et al.[5-8] applied the virtual synchronous generator (VSG) control strategy, which has the external characteristics of synchronous generator by controlling the inverter, to AC microgrid to enhance output damping. Although the hybrid energy storage system composed of batteries and supercapacitors can suppress the bus voltage fluctuation caused by the lack of inertia in the DC microgrid, the increase of the equivalent inertia of the system has higher requirements for energy storage capacity, which inevitably increasing costs of investment and maintenance[9-12]. Therefore, some effective control measures are adopted to improve the inertia of DC microgrid, so as to reduce the fluctuation of bus voltage and ensure the stable operation of the system[13-16]. However, the traditional control methods are limited to enhance the inertia of the system, which is not good for the improvement of power quality.

In view of the research idea of VSG control, the virtual DC generator (VDCG) control that can simulate the inertia characteristics of DC generator is proposed to buffer bus voltage because of the impact of disturbance[17-20], while the VDCG technology for renewable energy sources in DC microgrid is not widely studied. Cheng et al.[21] proposed a VDCG control method for PV power generation system

and applied to the hierarchical control of solar-storage DC microgrid, which forms an maximum power point tracking (MPPT) + VDCG control strategy to improve the stability and disturbance immunity of the system. In order to improve the inertia of the wind-storage DC microgrid, a two-stage control method that the front stage converter is controlled by MPPT or limited power technical control (LPTC) and the back stage converter is controlled by virtual DC generator is proposed to ensure the increase of inertia and output of maximum power[22]. He et al. [23] introduced virtual inertia to the power converter of renewable energy power generation unit to actively suppress the bus voltage fluctuation caused by intermittent power generation, but the influence of MPPT of solar-wind energy is not considered.

Based on the above analysis, an improved virtual DC generator control strategy for PV power generation unit is studied. The principle of virtual DC generator control with MPPT is analyzed, the small signal model is established, and the influence mechanism of inertia coefficient and damping coefficient on stability is analyzed. According to the root locus characteristics of virtual DC generator, the proposed method provides a theoretical reference for the optimal design of inertia coefficient and damping coefficient. Finally, the solar and energy storage DC microgrid system model is built, and the correctness and effectiveness of the proposed control strategy is verified by simulation.

1 Structure of DC microgrid system in railway field

This study only takes DC microgrid system composed of solar and storage energy in railway field as the research object, and the system is shown in Fig. 1. The system consists of photovoltaic power generation, storage battery unit and load.

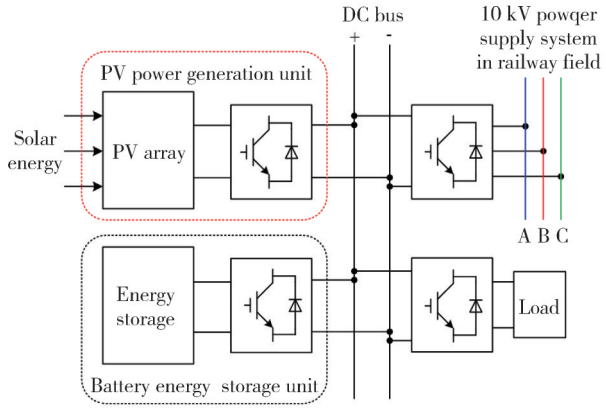

Fig. 1 System of solar-storage DC microgrid in railway field

The PV power generation unit with almost no inertia characteristics is composed of PV array, boost converter and virtual DC generator control module, and the topology is shown in Fig.2.

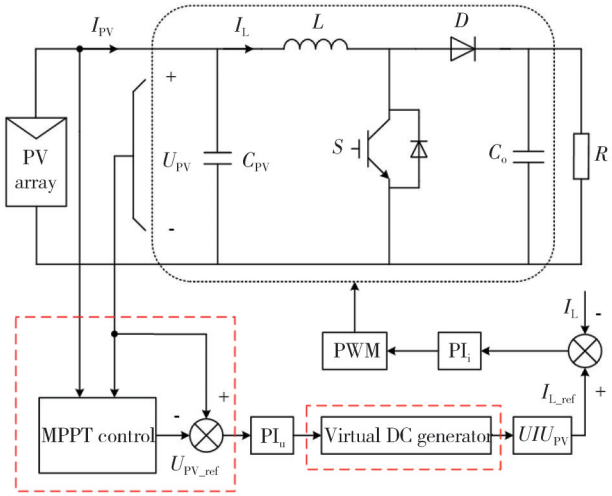

Fig. 2 Topology of PV power generation unit

2 Inertia control of DC microgrid in railway field

2.1 Inertia analysis of DC microgrid

The inertia is physically described as the inherent property of the object to resist the change of own motion state, which is an important guarantee for the stable operation of the system.

However, the inertia refers to the ability to resist the frequency mutations caused by external disturbances in AC system, providing sufficient time for the synchronous generator to readjust the active power. The inertia can be defined as

$$H_{AC}=\frac{W_r}{S_N}=\frac{1}{2}\frac{J\omega^2}{S_N}, \tag{1}$$

where H_{AC} is the inertia of the AC system, W_r is the kinetic energy stored by the rotor at rated speed, S_N is the rated capacity of the synchronous generator, J is the moment of inertia of the rotor, and ω is the rotor speed.

By analyzing the inertia of the AC system, The inertia of a DC system can be used to measure resistance to voltage mutations. The inertia of the DC system can be expressed as

$$H_{DC}=\frac{\sum W_{qi}}{\sum S_{Ni}}=\frac{\sum_{i=1}^{m}\frac{1}{2}C_iU^2}{\sum_{i=1}^{n}S_{Ni}}, \tag{2}$$

where H_{DC} is the inertia of the DC system, W_{qi} is the power energy stored by the capacitor, S_{Ni} is the rated capacity of the ith capacitor, C_i is the capacitance value,

and U is the value of capacitance voltage.

The inertia constant of DC microgrid refers to the time required to release all the energy stored by the capacitor at the rated voltage. In order to reduce the cost as much as possible, the capacity of the energy storage system and the capacity of the capacitor in the DC microgrid of practical engineering is small, which results in the low inertia characteristics of the system.

2.2 Improved virtual DC generator control

The energy of DC microgrid in the railway is transferred by stationary power electronic converters, resulting in low inertia of the system. Meanwhile, the DC link voltage will be greatly affected by the intermittence and fluctuation of solar energy. Therefore, the control strategy that the inertia can be simulated without increasing the energy storage capacity is adopted in this study to boost the stability. The mechanical and electromagnetic equations of DC generator are added into the control of boost converter to make it have the inertia and damping characteristics, which is able to improve the stability of the voltage.

The boost converter can be regarded as a two-port network, and the equivalent model of virtual DC generator control is shown in Fig.3.

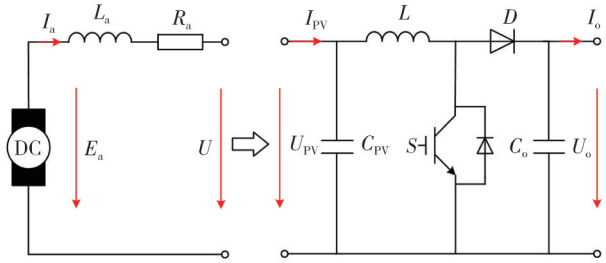

Fig. 3 Equivalent model of virtual DC generator control

According to the mechanical and electromagnetic equations of DC generator, the mathematical model of virtual DC generator control is defined as follows.

The mechanical equation is shown as

$$\begin{cases} T_{vm} - T_{ve} - D_{damp}(\omega - \omega_0) = J\dfrac{d\omega}{dt}, \\ T_{vd} = D_{damp}(\omega - \omega_0), \\ T_{viner} = J\dfrac{d\omega}{dt}, \end{cases} \tag{3}$$

where D_{damp} and J are the damping and inertia coefficients of the virtual DC generator, respectively; T_{vm} and T_{ve} are the virtual mechanical torque and electromagnetic torque, respectively; ω and ω_0 are the virtual actual angular velocity and rated angular velocity, respectively; P_{ve} represents the virtual electromagnetic power; T_{vd} and T_{viner} are the virtual mechanical torque varying with damping coefficient and the virtual mechanical torque varying with inertia coefficient, respectively.

The electromagnetic equation is shown as

$$\begin{cases} E_a = C_T\varphi\omega, \\ E_a = U + I_aR_a + L_a\dfrac{di_a}{dt}, \\ P_{ve} = E_aI_a, \end{cases} \tag{4}$$

where E_a is the induced electromotive force of the armature, C_T is the torque coefficient, φ is the magnetic flux, U is the terminal voltage of the DC generator, R_a is the equivalent resistance of the armature circuit, and I_a represents the armature current.

From Eqs. (3) and (4), it can be seen that the angular velocity will slowly change with J and D_{damp} when the virtual mechanical power P_{vm} changes suddenly, mitigating the change of virtual electromagnetic power P_{ve}. Therefore, the change of the output can be effectively reduced owing to the sudden change of the input.

The angular velocity and the induced electromotive force are adjusted by the mechanical and the electromagnetic equations of the virtual DC generator respectively to respond to the voltage disturbance caused by power fluctuation. The control block diagram of the virtual DC generator is shown in Fig.4.

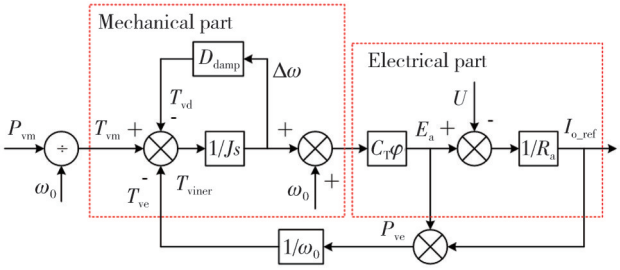

Fig. 4 Control block diagram of virtual DC generator

As shown in Fig.4, The mechanical part of the virtual DC generator is used to realize the balance of virtual torque and speed, and the electrical part transforms the speed balance into voltage balance to enhance the inertia of DC bus voltage. The voltage deviation can be eliminated by the virtual damping torque T_{vd}, and the oscillation can be suppressed by the virtual inertia torque T_{viner}.

The traditional control block diagram of PV boost converter is shown in Fig.5.

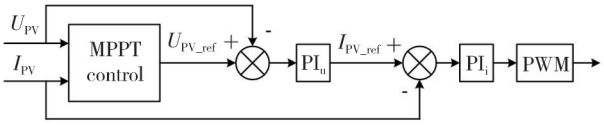

Fig. 5 Traditional control block diagram of PV boost converter

As can be seen from Fig.4, the virtual machine torque T_{vm} is adjusted by the virtual machine power P_{vm}, achieving stable output control. Therefore, the traditional control

block diagram of PV boost converter is introduced into the virtual DC generator to obtain the improved virtual DC generator control method. The improved control block diagram is shown in Fig.6.

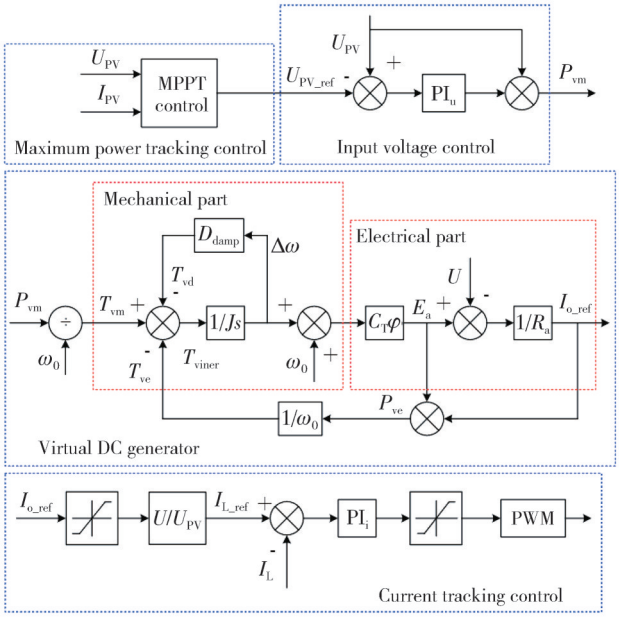

Fig. 6 Improved control block diagram of virtual DC generator

The improved virtual DC generator control is composed of maximum power tracking control, input voltage control, virtual DC generator, and current tracking control according to the control structure in Fig.6.

3 Small signal model based on improved VDCG control

3.1 Small signal model of PV boost converter

The switching network part will be replaced by an ideal transformer if the loss of switching devices is ignored in boost converter, and the average switching circuit model can be established, as shown in Fig.7.

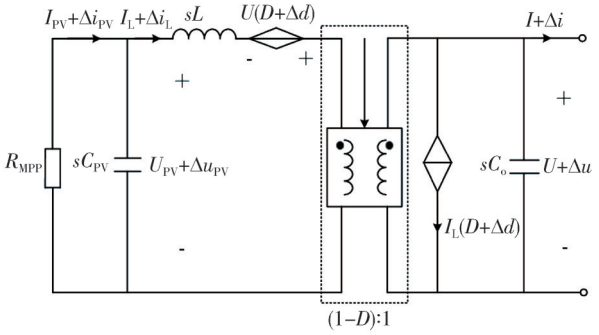

Fig. 7 Average switching circuit model of PV boost converter

According to the voltage and current relationship of the primary and secondary sides of the ideal transformer, the simplified average switching circuit model can be established, as shown in Fig.8.

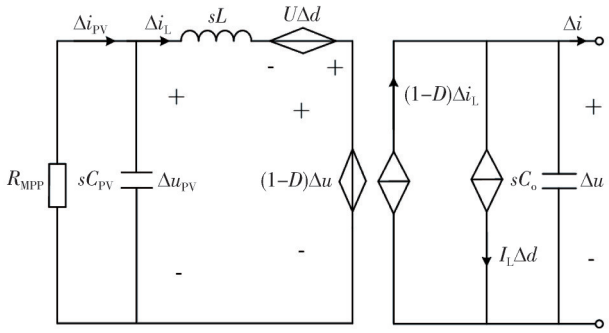

Fig. 8 Simplified average model of switching circuit

Then, the small signal model of PV boost converter can be obtained as

$$\begin{cases} sL\Delta i_L = \Delta u_{PV} + U\Delta d - (1-D)\Delta u, \\ sC_o\Delta u = (1-D)\Delta i_L - I_L\Delta d - \Delta i, \\ sC_{PV}\Delta u_{PV} = \Delta i_{PV} - \Delta i_L, \end{cases} \tag{5}$$

where U is the steady-state value of output voltage and I_L is the steady-state value of input current.

The transfer function can be obtained according to Eq. (4) as

$$G_{ui}^{PV}(s) = \frac{\Delta u_{PV}}{\Delta i} = -\frac{a_5}{a_1 s^3 - a_2 s^2 + a_3 s - a_4}, \tag{6}$$

$$G_{ud}(s) = \frac{\Delta u}{\Delta d} = -\frac{b_5 s^2 - b_6 s + b_7}{b_1 s^3 - b_2 s^2 + b_3 s - b_4}, \tag{7}$$

$$G_{id}(s) = \frac{\Delta i_L}{\Delta d} = \frac{c_5 s^2 + c_6 s - c_7}{c_1 s^3 - c_2 s^2 + c_3 s - c_4}, \tag{8}$$

$$G_{ud}^{PV}(s) = \frac{\Delta u_{PV}}{\Delta d} = -\frac{d_5}{d_1 s^3 - d_2 s^2 + d_3 s - d_4}, \tag{9}$$

$$A_{io}(s) = \frac{\Delta i_L}{\Delta i} = \frac{e_5 s - e_6}{e_1 s^3 - e_2 s^2 + e_3 s - e_4}, \tag{10}$$

$$Z_o(s) = \frac{\Delta u}{\Delta i} = \frac{f_5 s^2 - f_6 s + f_7}{f_1 s^3 - f_2 s^2 + f_3 s - f_4}. \tag{11}$$

The slope coefficient of the linearized U-I characteristic curve is shown as

$$k_{PV} = \frac{N_p I_{sc}}{\left[\exp\left(\frac{U_{oc}}{aU_t}\right) - 1\right] aN_s U_t} \exp\left(\frac{U_{PV}}{aN_s U_t}\right). \tag{12}$$

3.2 Small signal model of improved VDCG control

The output power of the virtual DC generator can be expressed as

$$P_{ve} = \frac{E_a - U_o}{R_a} E_a. \tag{13}$$

Substituting Eq. (4) into Eq. (13), the expression of P_{ve} can be deduced as

$$P_{ve} = \frac{C_T\varphi\omega - U_o}{R_a} C_T\varphi\omega = \frac{(C_T\varphi)^2\omega^2}{R_a} - \frac{U_o C_T\varphi\omega}{R_a}. \tag{14}$$

The expression of T_{ve} can be obtained from Eq. (14) as

$$T_{ve}=\frac{P_{ve}}{\omega}=\frac{\left(C_T\varphi\right)^2\omega}{R_a}-\frac{U_oC_T\varphi}{R_a}. \tag{15}$$

Let $\Delta\omega=\omega-\omega_0$, Eq. (3) can be rewritten as

$$T_{vm}-\frac{\left(C_T\varphi\right)^2\left(\omega_0+\Delta\omega-U_oC_T\varphi\right)}{R_a}-D\Delta\omega=J\Delta\dot{\omega}. \tag{16}$$

Assuming that a small perturbation is added into Eq. (16), the formula after disturbance separation and variable substitution can be expressed as

$$\hat{T}_{vm}-\frac{\left(C_T\varphi\right)^2\Delta\hat{\omega}}{R_a}-D\Delta\hat{\omega}=J\Delta\dot{\hat{\omega}}. \tag{17}$$

The transfer function of the virtual DC generator after Laplace transformation can be obtained as

$$G_{VDCG}(s)=\frac{1}{Js+\dfrac{C_T^2\varphi^2}{R_a}+D_{damp}}. \tag{18}$$

It can be seen from Eq. (18) that the virtual DC generator is approximately a first-order inertia link containing an energy storage element and the similar function is equivalent to paralleling a "virtual capacitor" with variable capacitance to the output side of PV boost converter. The capacitance of the "virtual capacitor" can be changed to effectively stabilize and buffer the disturbance of DC bus voltage by reasonably designing the inertia coefficient J and damping coefficient D_{damp} of the virtual DC generator, which can improve the power quality.

Thus, Eq. (5) can be expressed as

$$U=C_T\varphi\omega-I_aR_a-L_a\frac{\mathrm{d}i_a}{\mathrm{d}t}. \tag{19}$$

The relationship between output voltage deviation and angular velocity deviation is shown as

$$\frac{\partial U}{\partial\omega}=C_T\varphi. \tag{20}$$

Therefore, the small signal model control block diagram of virtual DC generator can be obtained, as shown in Fig.9.

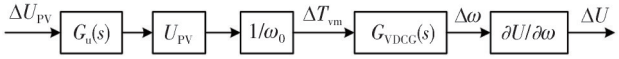

Fig. 9 Small signal model control block diagram of virtual DC generator

The transfer function of improved virtual DC generator control between the input voltage deviation and the output voltage deviation in the PV boost converter is shown as

$$G_1(s)=\frac{\Delta U(s)}{\Delta U_{PV}(s)}=\frac{C_T\varphi R_aU_{PV}G_u(s)}{\left(JR_as+C_T^2\varphi^2+R_aD_{damp}\right)\omega_0}. \tag{21}$$

Therefore, the block diagram of small signal model of PV boost converter with improved virtual DC generator control is shown in Fig.10.

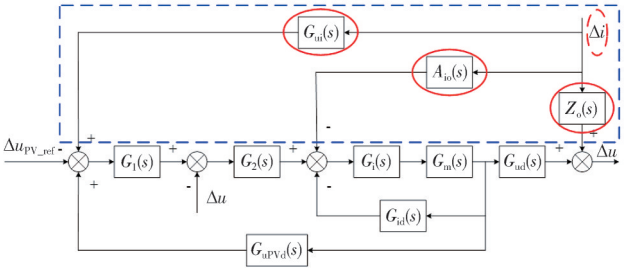

Fig. 10 Small signal model block diagram for improved VDCG control

If the influence of load mutation is ignored and the influence of PV power fluctuation in source side on the system is only considered to simplify the analysis, the effects of transfer functions $G_{ui}(s)$, $A_{io}(s)$ and $Z_o(s)$ can be ignored. The simplified control block diagram of small signal model is shown in Fig.11.

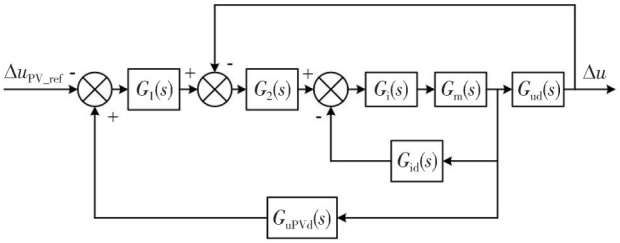

Fig. 11 Simplified control block diagram of improved VDCG

4 Small signal stability analysis of improved VDCG

As can be seen from Eq. (21), the inertia coefficient J and damping coefficient D_{damp} are only related to the $G_1(s)$. Therefore, the Bode diagram of $G_1(s)$ due to the change of J and D_{damp} can be drawn, as shown in Fig.12.

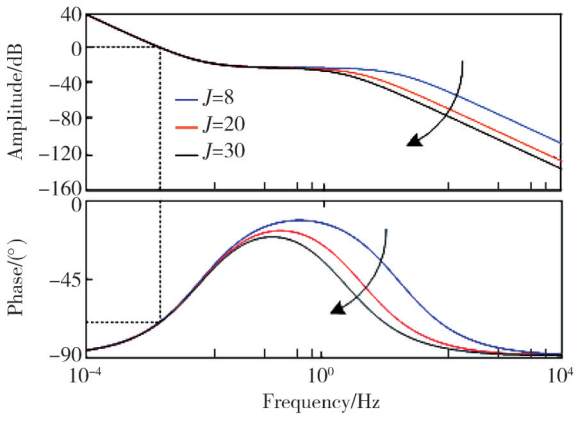

(a) Bode diagram of different inertia coefficients

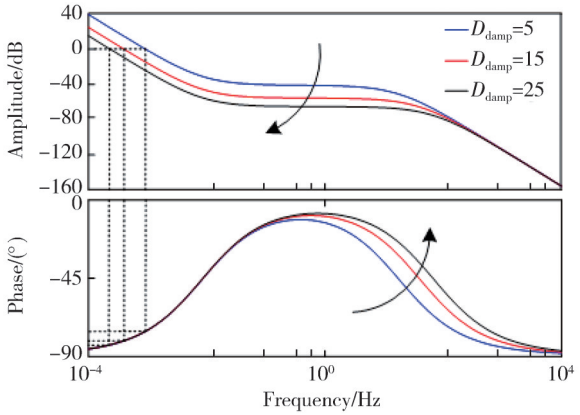

(b) Bode diagram of different damping coefficients

Fig. 12 Bode diagram of $G_1(s)$

It can be seen that the cut-off frequency and phase margin of the system will not be changed with of the increase of J when D_{damp} remains unchanged. Therefore, the value of J has no obvious influence on the stability of the system. As can be seen from Fig.12(b), the cut-off frequency and phase margin of the system will be decreased with the increase of D_{damp} when J remains unchanged. Since $G_1(s)$ is a second-order system and the amplitude margin is infinite at this time, the stability of the system will be reduced with the increase of D_{damp}.

The open-loop transfer function of the system can be obtained by the simplified small signal model block diagram of the improved virtual DC generator control.

$$G_{u\_op}(s)=\frac{-G_1(s)G_2(s)G_{ud}^{PV}(s)G_i(s)}{1+G_{id}(s)G_i(s)+G_2(s)G_{ud}(s)G_i(s)}, \quad (22)$$

$$G_2(s)=\frac{U}{U_{PV}R_a}. \quad (23)$$

The Bode diagram of the improved virtual DC generator control system can also be drawn by Eq. (22), and the influence of different rotational inertia coefficient J and damping coefficient D_{damp} on the system stability can be analyzed, as shown in Fig.13.

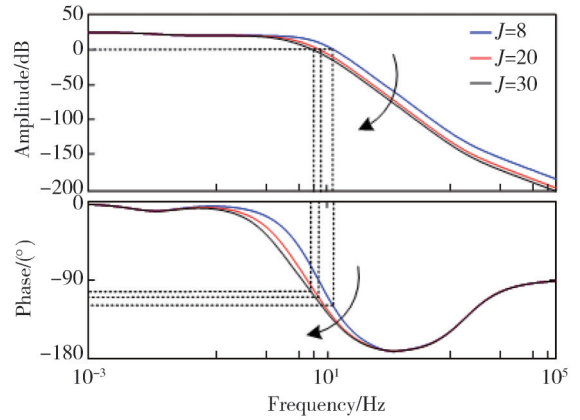

(a) Bode diagram of different inertia coefficients

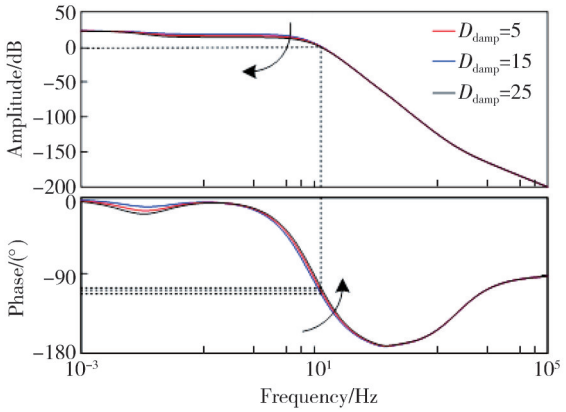

(b) Bode diagram of different damping coefficients

Fig. 13 Bode diagram of $G_{u\_op}(s)$

It can be seen from Fig.13(a) that the high frequency band of $G_{u\_op}(s)$ is mainly affected by J when D_{damp} is constant, and the phase angle margin of the system will enlarge owing to the increase of J, which diminishes the influence of disturbance signal on the system stability. It can be seen from Fig.13(b) that the low frequency band of $G_{u\_op}(s)$ is mainly affected by D_{damp} when J remains unchanged, and the phase angle margin of the system will increase slightly due to the enlargement of D_{damp}, which enhances the stability of the system.

Based on the above analysis, the inertia coefficient J and damping coefficient D_{damp} are two important parameters of the improved virtual DC generator control. In a certain range, the stability of the system can be effectively improved by different J and D_{damp}.

5 Simulation and discussion

According to the principle of the improved VDCG method, the simulation model of the PV and energy storage DC microgrid in railway field was built in Matlab/Simulink to verify the effectiveness and rationality of the proposed improved virtual DC generator control strategy. The main parameters are listed in Table 1.

Table 1 Simulation parameters of system

Parameter	Value
Input voltage U_{PV}/V	290
Equivalent resistance R_a/Ω	1
Rated angular velocity ω_0/(rad·s^{-1})	314
Input capacitance C_{PV}/μF	100
Input inductance L_{PV}/mH	1
DC bus voltage U/V	400
Sampling frequency f/kHz	10

In order to analyze the control effect of the improved virtual DC generator method, the simulation was carried out under the conditions of steady-state operation and PV power disturbance, respectively.

5.1 Simulation results under steady-state operation

The simulation model is operate under the condition that the ambient temperature remains unchanged at 25 ℃ and the irradiance is maintained at 1 000 $W \cdot m^{-2}$. The number of parallel modules is 4, and the number of serial modules is 10 in the PV arrays. The simulation waveforms of the steady-state operation are shown in Fig.14.

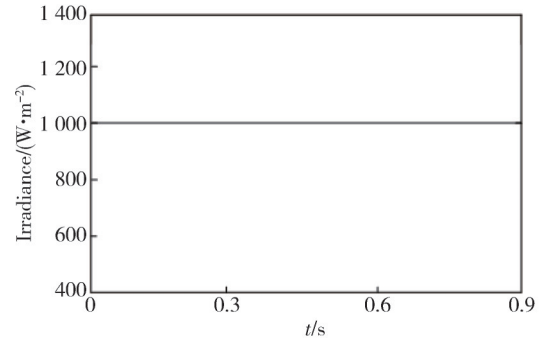

(a) Steady-state curve of light intensity

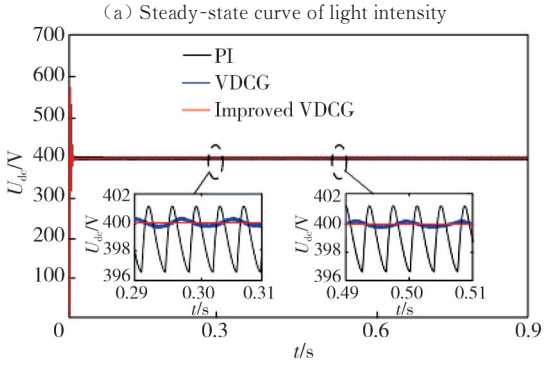

(b) Waveform of DC bus voltage

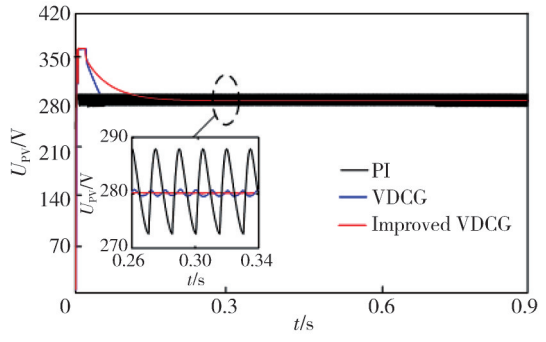

(c) Waveform of output voltage of PV unit

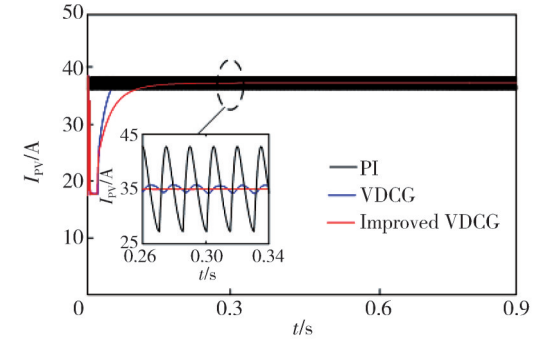

(d) Waveform of output current of PV unit

Fig. 14 Simulation results of stable illumination intensity

Fig. 14(a) is the irradiance curve of steady-state operation. It can be seen that the light intensity remains unchanged at 1 000 $W \cdot m^{-2}$. Fig. 14(b) shows the bus voltage waveform at stable irradiance. Compared with the traditional PI control, when the virtual DC generator control is adopted, the bus voltage changes more gently and the voltage fluctuation amplitude is smaller in the same time. However, the bus voltage is always stable at about 400 V after adopting the improved virtual DC generator control. It can be seen from Fig.14(c) and (d) that when the light intensity of PV unit remains stable, there are the fluctuations of the output voltage and current of the PV unit when the traditional PI control and virtual DC generator control are adopted. The variation ranges of output voltage and current of PV unit controlled by traditional PI are ΔU=8 V, ΔI=7 A, respectively. The variation ranges of output voltage and current of PV unit controlled by virtual DC generator are ΔU=2 V, ΔI=1 A, respectively. However, the output voltage and current of the PV unit controlled by the improved virtual DC generator have no change.

The above simulation results show that the improved virtual DC generator control can effectively suppress the voltage fluctuation of DC bus, which enhances the system inertia and improves the stability of the system.

5.2 Simulation results with PV power disturbance

When the light changes, the PV power fluctuates. The simulation results PV are shown in Fig.15.

Fig. 15(a) shows the change of light intensity that decreases from 1 000 $W \cdot m^{-2}$ to 400 $W \cdot m^{-2}$ at 0.3 s, increases from 400 $W \cdot m^{-2}$ to 800 $W \cdot m^{-2}$ at 0.5 s, and increases from 800 $W \cdot m^{-2}$ to 1 000 $W \cdot m^{-2}$ at 0.7 s. Due to the sudden change of light intensity, the output power is prone to sudden change, which impacts the bus voltage. Compared with the traditional PI control, it can be seen from Fig.15(b) that when the virtual DC generator control is adopted, the DC bus voltage causes a downward spike with a change value of 5 V because of the sudden weakening of the light at 0.3 s. While there is also an upward voltage mutation of 2 V on account of the sudden enhancement of the light at 0.5 s and 0.7 s. By using the improved virtual DC generator control, the downward voltage peak is reduced to 3 V and the upward voltage change is reduced to 0.5 V, which effectively improves the system stability. As can be seen from Figs.15(c) and 15(d), the virtual DC generator control enhances the system inertia and the influence of PV power fluctuation is effectively weakened. After adding the improved virtual DC generator control, the system inertia is further improved, which not only slows down the change of output voltage, but also reduces the peak value.

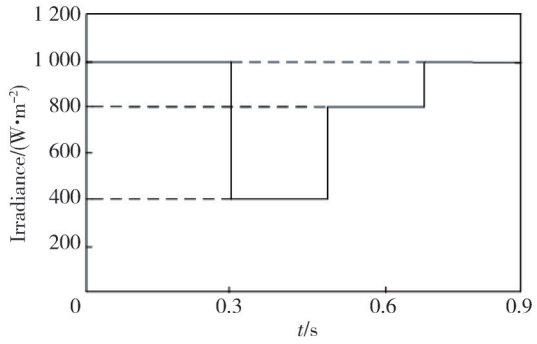

(a) Sudden change curve of light intensity

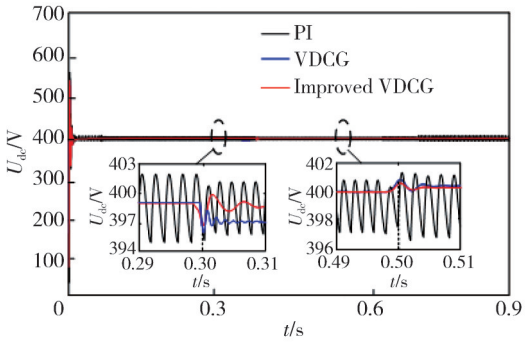

(b) Waveform of DC bus voltage

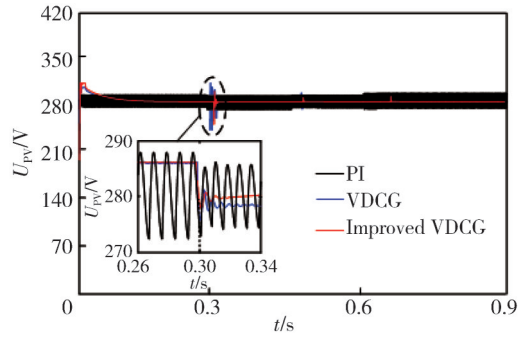

(c) Waveform of output voltage for photovoltaic unit

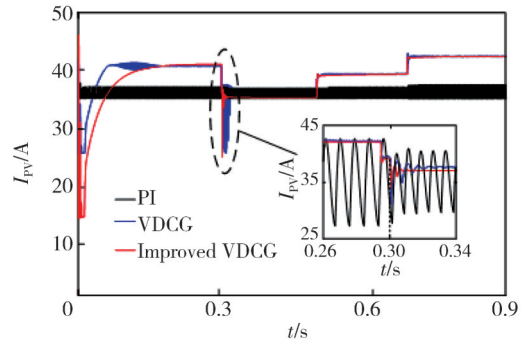

(d) Waveform of output current for photovoltaic unit

Fig. 15 Simulation results with PV power disturbance

6 Conclusions

Aiming at the PV power fluctuation and the low inertia and weak damping characteristics of a DC microgrid system composed of PV and energy storage in railway field, an improved control strategy based on virtual DC generator was proposed. The mechanical equation and electromagnetic equation of DC generator were added to the control link of the interface converter of PV power generation unit, and the influence of PV MPPT was considered to enhance the inertia and damping of PV power generation unit. Based on the small signal modeling of improved virtual DC generator control, the influence of different inertia coefficients and damping coefficients on system stability was analyzed. By analyzing the simulation results, the following conclusions are obtained.

1) Considering the influence of PV MPPT, the virtual DC generator is added into the control of PV interface converter to increase the inertia of PV power generation unit, which provides a certain inertia support for the system.

2) Compared with the traditional PI control, the virtual DC generator control strategy that simulates the inertia and damping characteristics of DC generator can effectively buffer and restrain the influence of power fluctuations on the bus voltage in a stable light intensity. But the improved virtual DC generator control strategy improves the system stability.

3) When the light intensity changes suddenly, there is an impact on the system because of the inertia free system for PV power generation system. The virtual DC generator control is adopted to weaken the influence of power fluctuation on bus voltage. However, the improved virtual DC generator control strategy can further increase the inertia of system, which improves the quality of the bus voltage.

Acknowledgement

This work was supported by National Natural Science Foundation of China (No. 52067013), Natural Science Foundation of Gansu Province (No. 20JR5RA395), and Tianyou Innovation Team of Lanzhou Jiaotong University (No. TY202010).

Declaration of conflicting interests

The authors have no conflict of interests related to this publication.

References

[1] HU H T, CHEN J Y, GE Y B, et al. Research on regenerative braking energy storage and utilization technology for high-speed railways. Proceedings of the CSEE, 2020, 40(1): 246-391.

[2] LI X L, GUO L, WANG C S, et al. Key technologies of DC microgrids: an overview. Proceedings of the CSEE,

2016, 36(1): 2-17.

[3] ZHU X R, HAN D H, MENG F Q, et al. Grid converter series virtual impedance method for improving DC microgrid stability. Power System Technology, 2019, 43(12): 4523-4531.

[4] ZHENG T W, CHEN L J, LIU W, et al. Multi-mode operation control for photovoltaic virtual synchronous generator considering the dynamic characteristics of primary source. Proceedings of the CSEE, 2017, 37(2): 454-464.

[5] CHOOPANI M, HOSSEINIAN S H, VAHIDI B. New transient stability and LVRT improvement of multi-VSG grids using the frequency of the center of inertia. IEEE Transactions on Power Systems, 2020, 35(1): 527-538.

[6] CHAI J Y, ZHAO Y Y, SUN X D, et al. Application and prospect of virtual synchronous generator in wind power generation system. Automation of Electric Power Systems, 2018, 42(9): 17-68.

[7] ALIPOOR J, MIURA Y, ISE T. Stability assessment and optimization methods for microgrid with multiple VSG units. IEEE Transactions on Smart Grid, 2018, 9(2): 1462-1471.

[8] ZHU Z B, ZHANG C Y, ZENG X B. Photovoltaic energy storage microgrid system based on adaptive rotating inertia VSG control strategy. Proceedings of the CSU-EPSA, 2021, 33(3): 67-72.

[9] RAVADA B R, TUMMURU N R. Control of a supercapacitor, battery and PV based stand-alone DC microgrid. IEEE Transactions on Energy Conversion, 2020, 35(3): 1268-1277.

[10] MANANDHAR U, WANG B, ZHANG X, et al. Joint control of three-level DC–DC converter interfaced hybrid energy storage system in DC microgrids. IEEE Transactions on Energy Conversion, 2019, 34(4): 2248-2257.

[11] E Z J, WANG G L, LI Z B, et al. Optimization control method for hybrid energy storage system to enhance the renewable energy absorption level of power grid. Proceedings of the CSU-EPSA, 2021, 33(3): 132-137.

[12] AUGUSTINE S, MISHRA M K. A unified control scheme for a standalone solar-PV low voltage DC microgrid system with HESS. IEEE Journal of Emerging and Selected Topics in Power Electronics, 2020, 8(2): 1351-1360.

[13] LI X L, GUO L, WANG C S, et al. Robust and autonomous DC bus voltage control and stability analysis for a DC microgrid//IEEE 8th International Power Electronics and Motion Control Conference, May 22-26, 2016, Hefei, China. New York: IEEE, 2016: 3708-3714

[14] GAVRILUTA C, CANDELA J I, ROCABERT J, et al. Adaptive droop for control of multiterminal DC bus integrating energy storage. IEEE Transactions on Power Delivery, 2015, 30(1): 16-24.

[15] ZHI N, ZHANG H. Improved hierarchical control strategy for DC microgrid. High Voltage Engineering, 2016, 42(4): 1316-1325.

[16] WANG C S, LI X L, GUO L, et al. A nonlinear disturbance observer based DC bus voltage control for a hybrid AC/DC microgrid. IEEE Transactions on Power Electronics, 2014, 29(11): 6162-6177.

[17] ZHANG H, ZHANG K T, XIAO X, et al. Control strategy of energy storage converter for simulating DC generator characteristics. Automation of Electric Power Systems, 2017, 41(20): 126-132.

[18] ZHANG X Y, LI H, FU Y. Dynamic stability analysis and self-adaptive voltage inertia control of DC microgrids with novel virtual machine. High Voltage Engineering, 2021, 47(8): 2865-2874.

[19] ZHI N, DING K, DU L, et al. An SOC-based virtual DC machine control for distributed storage systems in DC microgrids. IEEE Transactions on Energy Conversion, 2020, 35(3): 1411-1420.

[20] SAMANTA S, MISHRA J P, ROY B K. Virtual DC machine: an inertia emulation and control technique for a bidirectional DC-DC converter in a DC microgrid. IET Electric Power Applications, 2018, 12(6): 874-884.

[21] CHENG Q M, YANG X L, CHU S Y, et al. Research on control strategy of PV system based on virtual DC generator. High Voltage Engineering, 2017, 43(7): 2097-2104.

[22] MA Y C, WANG S T, LIU G C, et al. Research on virtual DC generator-based control strategy of DC microgrid with wind/energy storage. High Voltage Engineering, 2020, 46(11): 3819-3831.

[23] HE F Q, LI Z Y, YANG R F, et al. Active virtual DC generator technique for new-energy unit of offshore platform. Ship Engineering, 2020, 42(10): 90-96.

铁路领域光伏发电单元改进的虚拟直流发电机技术

赵 峰, 肖成锐*, 陈小强, 王 英

兰州交通大学 自动化与电气工程学院, 甘肃 兰州 730070

摘 要: 针对铁路领域中光伏等新能源构成的电力电子化直流微网系统存在低惯量、弱阻尼特性, 以及光伏功率波动易引起直流微网母线电压大幅波动的问题, 考虑在光伏发电单元的接口变换器中采用虚拟直流发电机技术, 使其具有直流发电机运行特性, 从而提高直流微网系统的惯性。此外, 传统的虚拟直流发电机控制没有考虑光伏最大功率跟踪的影响, 为此, 提出一种改进的虚拟直流发电机控制策略。通过建立小信号模型进一步分析惯量系数、阻尼系数对系统稳定性的影响。仿真结果表明, 该控制策略有效减弱了光伏功率波动对直流母线电压的影响, 增强了系统稳定性, 从而验证了该方法的可行性和有效性。

关键词: 可再生能源; 光伏发电系统; 电力电子化直流微网系统; 虚拟直流发电机控制; 虚拟惯性

引用格式: ZHAO Feng, XIAO Chengrui, CHEN Xiaoqiang, et al. Improved virtual DC generator technique for PV power generation units in railway field. Journal of Measurement Science and Instrumentation, 2025, 16(3): 415-424. DOI: 10.62756/jmsi.1674-8042.2025040